Steel and Composite Structures, *Vol. 35, No. 6 (2020) 765-777*
DOI: https://doi.org/10.12989/scs.2020.35.6.765

Nonlinear forced vibrations of multi-scale epoxy/CNT/fiberglass truncated conical shells and annular plates via 3D Mori-Tanaka scheme

Seyed Sajad Mirjavadi[1], Masoud Forsat*[2], Mohammad Reza Barati[3] and AMS Hamouda[1]

[1]*Department of Mechanical and Industrial Engineering, Qatar University, P.O. Box 2713, Doha, Qatar*
[2]*Department of Civil and Architectural Engineering, Qatar University, Doha, Qatar*
[3]*Fidar project Qaem Company, Darvazeh Dolat, Tehran, Iran*

(*Received March 7, 2020, Revised May 19, 2020, Accepted May 23, 2020*)

Abstract. In the context of classic conical shell formulation, nonlinear forced vibration analysis of truncated conical shells and annular plates made of multi-scale epoxy/CNT/fiberglass composites has been presented. The composite material is reinforced by carbon nanotube (CNT) and also fiberglass for which the material properties are defined according to a 3D Mori-Tanaka micromechanical scheme. By utilizing the Jacobi elliptic functions, the frequency-deflection curves of truncated conical shells and annular plates related to their forced vibrations have been derived. The main focus is to study the influences of CNT amount, fiberglass volume, open angle, fiber angle, truncated distance and force magnitude on forced vibrational behaviors of multi-scale truncated conical shells and annular plates.

Keywords: forced vibration; annular plate; conical shell; multi-scale composite; carbon nanotube; annular sector

1. Introduction

Scholars are always trying to accomplish more comfortable life for human and to establish modern applied sciences. Thus, the requirement for smart and advanced materials has grown, and existent technologies are frequently exchanged by progressive technologies (Feng *et al*. 2017, Zhang *et al.* 2017, Dong *et al*. 2018, Safaei *et al*. 2019, Mirjavadi *et al*. 2017, 2018, 2019, Azimi *et al*. 2017, 2018). A polymeric material has already replaced ordinary materials including metals and ceramics because of its low weight, easy manufacturing, and low costs (Thanh *et al.* 2019, Ahmed *et al.* 2019). Therewith, a polymer possesses prominent corrosion stability and promising mechanical character. But, there are some disadvantages related to polymeric components, including slight thermal stability, downscale stiffness and environmental stability. In order to eschew such sorts of disadvantages, polymeric composites were manufactured via reinforcement of matrices based on an extensive range of filler materials (Vo *et al*. 2017, Houari *et al.* 2018, Kaci *et al.* 2018). According to the desirable performances of the conclusive material, the polymeric matrix may be reinforced via different kinds of macro to nano size fillers including fibers, particles and even platelets (Wu *et al.* 2017, Zhao *et al*. 2017). The performances of produced composite rely on the properties of both host material and filler. However, the performances of polymeric materials will decrease by passing time because of diverse factors including subjecting to UV, high temperatures or moisture. Composites which contain polymeric matrix and fiber reinforcement are produced to prevail such problems and enhance the overall performances of composite materials.

Fibers in reinforced polymeric materials represent remarkable characteristics including desired flexibility, aspect ratio and stability while the matrix defends the fibers against unfair conditions and retains their location. Nowadays, diverse sorts of artificial and synthetic fibers have been employed for reinforcing the polymeric matrices and then improving the performances of the final product. Such reinforced composites are applied in a variety of engineering fields such as aerospace, ocean and even automobiles, owning to the their desired cost and weight together with notable strength. For improving the out-of-plane performances of a composite, more than one filler element is needed. Note that weight is a very vital parameter in several applications including space vehicles and automobiles, and large size fillers yield higher to weights. Accordingly, nano scale fillers are often prior to macro scale counterparts. Multiple investigations have proved the elevated mechanical, thermal, and electrical characteristics of a nanoparticle reinforced composite. An advanced composite made from embedded fibers and reinforcing nano-dimension fillers (graphene, carbon nanotube, ant etc.) is introduced as a multi-scale composite (Marynowski 2017, Wattanasakulpong and Chaikittiratana 2015, Barati and Zenkour 2017). Such kind of composite is also defined as a multi-function composite due to possessing conventional load-sharing character of fiber reinforced material and also the extra functional characteristics (stiffness, strength, conductivity) related to the specific nanomaterials.

According to recent studies, the multi-scale composite can be modeled via several approaches including Halpin-Tsai and Eshelby-Mori-Tanaka forms (Mori and Tanaka

*Corresponding author, Ph.D.
E-mail: masoudforsatlar@gmail.com

ISSN: 1229-9367 (Print), 1598-6233 (Online)

1973). Although the Eshelby–Mori–Tanaka approach has high efficacy for multi-scale material modeling, it sometimes yields an asymmetric stiffness tensor for the composites, whereas, the 3D Mori-Tanaka's stiffness tensor, is always symmetric (Kazakov *et al*. 2019). The later can be used as an efficient tool for elastic properties definition of multi-scale composite. Also, there are many publications on vibration analysis of multi-scale composite structures, there is no investigation on nonlinear vibrations of annular sectors made of hybrid epoxy/fiberglass/CNT material.

It must be stated that annular plates possess remarkable applications in diverse engineering sections including defense industry, semi-conductors, space vehicle, chemical plants and bio-medical sectors. Recently, few studies are devoted to examine mechanical characteristics of annular plates made of composite materials. Dai *et al.* (2019) examined vibrational behavior of annular plates reinforced by functional gradation of nanotubes in hygro-thermal environments. An investigation on vibrations of graphene reinforced annular plates is performed by Liu *et al.* (2019). Also, Keleshteri *et al.* (2019) studied nonlinear bending behavior of carbon nanotube reinforced annular plates with variable thickness. Safarpour *et al.* (2020) researched linear vibrations of graphene reinforced annular plates based on a numerical approach. Based on a higher order theory, Wang *et al.* (2020) researched free vibrations of graphene reinforced annular plates under thermal load. According to the best of our knowledge, nonlinear forced vibrations of multi-scale epoxy/CNT/fiberglass annular sector plates under external harmonic loads is not studied before.

Different plate and shell theories are available in the literature (Abualnour *et al.* 2019, Addou *et al*. 2019, Balubaid *et al.* 2019, Batou *et al.* 2019, Bellal *et al.* 2020, Berghouti *et al.* 2019, Bouamoud *et al.* 2019, Bourada *et al.* 2019, Boussoula *et al.* 2020, Boutaleb *et al.* 2019, Chaabane et al. 2019, Draiche *et al.* 2019, Draoui *et al.* 2019, Hellal *et al*. 2019, Hussain *et al.* 2019, Kaddari *et al.* 2020, Khiloun *et al*. 2019, Medani *et al*. 2019, Meksi *et al*. 2019, Refrafi *et al.* 2020, Rahmani *et al*. 2020, Sahla *et al.* 2019, Semmah *et al.* 2019, Soltani et al. 2019, Tlidji *et al.* 2019, Tounsi *et al*. 2020, Zarga *et al*. 2019, Zaoui *et al*. 2019). In the context of classic conical shell formulation, nonlinear forced vibration analysis of truncated conical shells and annular plates made of multi-scale epoxy/CNT/fiberglass composites has been presented. The composite material is reinforced by carbon nanotube (CNT) and also fiberglass for which the material properties are defined according to a 3D Mori-Tanaka micromechanical scheme. By utilizing the Jacobi elliptic functions, the frequency-deflection curves of truncated conical shells and annular plates related to their forced vibrations have been derived. The main focus is to study the influences of CNT amount, fiberglass volume, open angle, fiber angle, truncated distance and force magnitude on forced vibrational behaviors of multi-scale truncated conical shells and annular plates.

2. Properties of multi-scale CNT/fiberglass/epoxy composite

In this research, a 3D Mori-Tanaka model is employed for evaluating multi-scale material properties. Also, all of glass fibers are assumed to have uni-directional alignment and CNTs have random diffusion (Fig. 1). The first issue is calculating material properties of a nano-composite (epoxy+ CNTs) which are elastic moduli (E_{11}, E_{22}), shear moduli (G_{12}, G_{23}) and bulk modulus (K_{23}) as (Kazakov *et al.* 2019)

$$\frac{E_{11}}{E_m}=\frac{1}{1+V_{cnt}\left(A_1+2\mu_m A_2\right)/\tilde{A}} \tag{1}$$

$$\frac{E_{22}}{E_m}=\frac{1}{1+V_{cnt}\left(\left(1-\mu_m\right)A_4-2\mu_m A_3+\left(1+\mu_m\right)A_5\tilde{A}\right)/2\tilde{A}} \tag{2}$$

$$G_{12}=G_m+\frac{G_m V_{cnt}}{\frac{G_m}{\Delta G}+2\left(1-V_{cnt}\right)S_{1212}} \tag{3}$$

$$G_{23}=G_m+\frac{G_m V_{cnt}}{\frac{G_m}{\Delta G}+2\left(1-V_{cnt}\right)S_{2323}} \tag{4}$$

$$K_{23}=\frac{\left(G_m+\lambda_m\right)\left(1+\mu_m\right)\left(1-2\mu_m\right)}{1-\mu_m\left(1+2\mu_{12}\right)+\frac{V_{cnt}}{\tilde{A}}\left(2\left(\mu_{12}-\mu_m\right)A_3+\left(1-\mu_m\left(1+2\mu_{12}\right)\right)A_4\right)} \tag{5}$$

in which $\Delta G=G_{cnt}-G_m$; G_{cnt} and G_m denote nanotube and matrix shear modulus, respectively. In addition, E_m and μ_m denote Young's modulus and Poisson ratio of matrix material; V_{cnt} defines CNT volume fraction which is associated with CNTs weight fraction (W_{cnt}), matrix density (ρ_m) and CNT density (ρ_{cnt}) as

$$V_{cnt}=\frac{W_{cnt}\rho_m}{\left(1-W_{cnt}\right)\rho_{cnt}+W_{cnt}\rho_m} \tag{6}$$

Moreover, the parameters A_i (i=1, 2, 3, 4, 5) should be determined by

$$\begin{aligned}
&A_1=D_1\left(B_4+B_5\right)-2B_2,\ \ A_2=\left(1+D_1\right)B_2-\left(B_4+B_5\right),\\
&A_3=B_1-D_1B_3,\ \ A_4=\left(1+D_1\right)B_1-2B_3,\\
&A_5=\frac{1-D_1}{B_4-B_5},\\
&\tilde{A}=2B_2B_3-B_1\left(B_4+B_5\right)
\end{aligned} \tag{7}$$

Next, the parameters in above relations may be defined as

$$\begin{aligned}
&B_1=V_{cnt}D_1+D_2+\left(1-V_{cnt}\right)\left(D_1S_{1111}+2S_{2211}\right),\\
&B_2=V_{cnt}+D_3+\left(1-V_{cnt}\right)\left(D_1S_{1122}+S_{2222}+S_{2233}\right),\\
&B_3=V_{cnt}+D_3+\left(1-V_{cnt}\right)\left(S_{1111}+\left(1+D_1\right)S_{2211}\right),\\
&B_4=V_{cnt}D_1+D_2+\left(1-V_{cnt}\right)\left(S_{1122}+D_1S_{2222}+S_{2233}\right),\\
&B_5=V_{cnt}+D_3+\left(1-V_{cnt}\right)\left(S_{1122}+S_{2222}+D_1S_{2233}\right)
\end{aligned} \tag{8}$$

in which S_{ijkl} denote the components of Eshelby's tensor which are introduced in the Appendix and

$$\begin{aligned}
&D_1=1+2\frac{G_{cnt}-G_m}{\lambda_{cnt}-\lambda_m},\\
&D_2=\frac{\lambda_m+2G_m}{\lambda_{cnt}-\lambda_m},\\
&D_3=\frac{\lambda_m}{\lambda_{cnt}-\lambda_m}
\end{aligned} \tag{9}$$

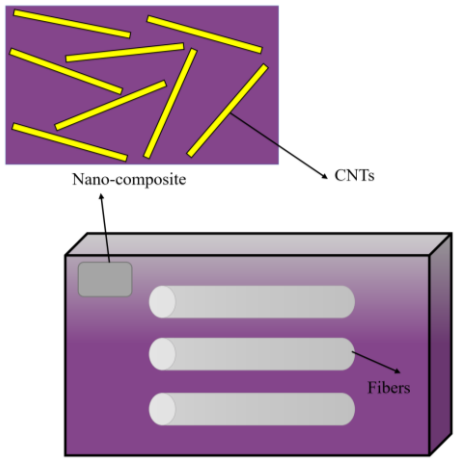

Fig. 1 Ingredients of reinforced multi-scale composites

It must be stated that λ_m and λ_{cnt} define Lame's constants of matrix and CNT, respectively determined by

$$\lambda_m = \frac{\mu_m E_m}{(1-2\mu_m)(1+\mu_m)}, \quad \lambda_{cnt} = \frac{\mu_{cnt} E_{cnt}}{(1-2\mu_{cnt})(1+\mu_{cnt})} \tag{10}$$

Next, it must be stated that the nano-composite material has below definitions for the bulk modulus $\hat{K}$ and shear modulus $\hat{G}$ as

$$\hat{K} = \frac{E_{11} + 4(1+\mu_{12})^2 K_{23}}{9} \tag{11}$$

$$\hat{G} = \frac{E_{11} + (1-2\mu_{12})^2 K_{23} + 6(G_{12}+G_{23})}{15} \tag{12}$$

In the case of multi-scale materials, the nano-composite part is defined as host material (matrix) and the glass fibers are macro scale fillers. Therefore, Young's modulus $\hat{E}$ and Poisson ratio $\hat{\mu}$ of host material are defined as

$$\hat{E} = \frac{9\hat{G}\hat{K}}{3\hat{K}+\hat{G}}, \quad \hat{\mu} = \frac{\hat{E}}{2\hat{G}} - 1 \tag{13}$$

For incorporating the effect of glass fiber as infinite filler with $\alpha \to \infty$, Eqs.(1)-(5) may be employed again. However, these equations should be modified by considering fiber volume fraction (V_f) instead of V_{cnt} and also all properties related to nano-composite material should be considered as the properties of matrix material. Also, all properties of the ingredients are presented in Table 1.

3. Truncated conical shell formulation

Having semi-vertex angle (β) and truncated distance (ξ_0), a truncated conical shell in coordinate system (ξ_1, ξ_2, ξ_3) has been illustrated in Fig. 2. Possible geometries as case studies for the truncated conical shell and annular plate (β=π/2) are shown in Fig. 3. For a thin annular plate or conical shell, components of strain field are (Barati and Zenkour 2019)

$$\begin{aligned} \varepsilon_{\xi_1} &= \varepsilon^0_{\xi_1} - z\chi_{\xi_1}, \\ \varepsilon_{\xi_2} &= \varepsilon^0_{\xi_2} - z\chi_{\xi_2}, \\ \gamma_{\xi_1\xi_2} &= \gamma^0_{\xi_1\xi_2} - 2z\chi_{\xi_1\xi_2}. \end{aligned} \tag{14}$$

in which

$$\begin{aligned} \varepsilon^0_{\xi_1} &= \frac{\partial u}{\partial \xi_1} + \frac{1}{2}\left(\frac{\partial w}{\partial \xi_1}\right)^2, \\ \varepsilon^0_{\xi_2} &= \frac{1}{\xi_1 \sin\beta}\frac{\partial v}{\partial \xi_2} + \frac{u}{\xi_1} + \frac{w}{\xi_1}\cot\beta \\ &+ \frac{1}{2\xi_1^2 \sin^2\beta}\left(\frac{\partial w}{\partial \xi_2}\right)^2, \\ \gamma^0_{\xi_1\xi_2} &= \frac{1}{\xi_1 \sin\beta}\frac{\partial u}{\partial \xi_2} + \frac{\partial v}{\partial \xi_1} - \frac{v}{\xi_1} \\ &+ \frac{1}{\xi_1 \sin\beta}\frac{\partial w}{\partial \xi_1}\frac{\partial w}{\partial \xi_2}, \\ \chi_{\xi_1} &= \frac{\partial^2 w}{\partial \xi_1^2}, \\ \chi_{\xi_2} &= \frac{1}{\xi_1}\frac{\partial w}{\partial \xi_1} + \frac{1}{\xi_1^2 \sin^2\beta}\frac{\partial^2 w}{\partial \xi_2^2}, \\ \chi_{\xi_1\xi_2} &= \frac{1}{\xi_1 \sin\beta}\frac{\partial^2 w}{\partial \xi_1 \partial \xi_2} - \frac{1}{\xi_1^2 \sin\beta}\frac{\partial w}{\partial \xi_2}. \end{aligned} \tag{15}$$

Table 1 Material properties of hybrid multi-scale composite material (Kazakove *et al.* 2019)

Material property	Value
Young modulus of matrix (E_m)	3.45 GPa
Young modulus of CNTs (E_{cnt})	1 TPa
Young modulus of fiberglass (E_f)	73.1 GPa
Density of matrix (ρ_m)	1270 kg/m^3
Density of CNTs (ρ_{cnt})	110 kg/m^3
Poisson's ratio of the matrix (μ_m)	0.35
Poisson's ratio of the CNTs (μ_{cnt})	0.17
Poisson's ratio of the fiberglass (μ_f)	0.22

(a) truncated conical shell

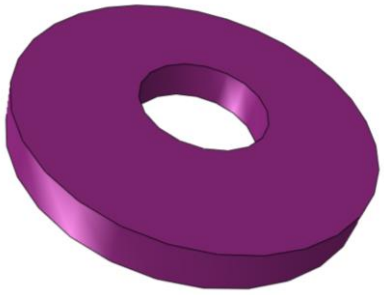

(b) annular plate

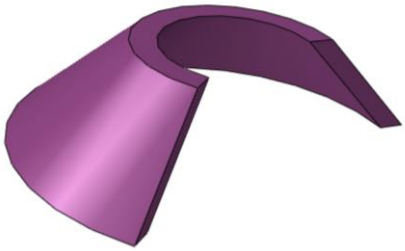

(c) truncated conical shell segment

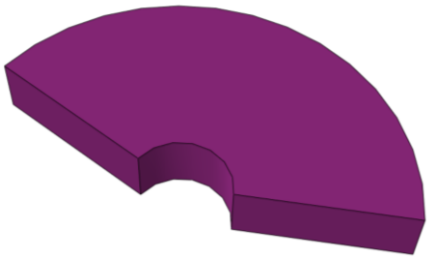

(d) annular plate sector

Fig. 3 The geometries of truncated conical shells and annular plates

Sector deflection is denoted by w and in-plane displacements are denoted by u and v. As mentioned, the conical shell and annular sector are made of fiber-reinforced multi-scale material for which the stresses σ_p (p= ξ_1, ξ_2, $\xi_1\xi_2$) can be determined as

$$\begin{Bmatrix}\sigma_{\xi_1}\\ \sigma_{\xi_2}\\ \sigma_{\xi_1\xi_2}\end{Bmatrix}=\begin{pmatrix}\tilde{Q}_{11} & \tilde{Q}_{12} & \tilde{Q}_{16}\\ \tilde{Q}_{12} & \tilde{Q}_{22} & \tilde{Q}_{26}\\ \tilde{Q}_{16} & \tilde{Q}_{26} & \tilde{Q}_{66}\end{pmatrix}\begin{Bmatrix}\varepsilon_{\xi_1}\\ \varepsilon_{\xi_2}\\ \gamma_{\xi_1\xi_2}\end{Bmatrix} \tag{16}$$

in which $\tilde{Q}_{ij}$ may be introduced by

$$\begin{aligned}
&\tilde{Q}_{11}=Q_{11}(\cos\theta)^4\\
&+2(Q_{12}+2Q_{66})(\sin\theta)^2(\cos\theta)^2\\
&+Q_{22}(\sin\theta)^4,\\
&\tilde{Q}_{12}=(Q_{11}+Q_{22}-4Q_{66})(\sin\theta)^2(\cos\theta)^2\\
&+Q_{12}\left((\sin\theta)^4+(\cos\theta)^4\right),\\
&\tilde{Q}_{16}=(Q_{11}-Q_{12}-2Q_{66})(\sin\theta)(\cos\theta)^3\\
&+(Q_{12}-Q_{22}+2Q_{66})(\sin\theta)^3(\cos\theta),\\
&\tilde{Q}_{22}=Q_{11}(\sin\theta)^4\\
&+2(Q_{12}+2Q_{66})(\sin\theta)^2(\cos\theta)^2\\
&+Q_{22}(\cos\theta)^4,\\
&\tilde{Q}_{26}=(Q_{11}-Q_{12}-2Q_{66})(\sin\theta)^3(\cos\theta)\\
&+(Q_{12}-Q_{22}+2Q_{66})(\sin\theta)(\cos\theta)^3,\\
&\tilde{Q}_{66}=(Q_{11}+Q_{22}-2Q_{12}-2Q_{66})(\sin\theta)^2(\cos\theta)^2\\
&+Q_{66}\left((\sin\theta)^4+(\cos\theta)^4\right).
\end{aligned} \tag{17}$$

where θ denotes orientation of fibers about ξ_1-axis and

$$\begin{aligned}
&Q_{11}=\frac{E_{11}}{1-\mu_{12}\mu_{21}},\quad Q_{12}=\frac{\mu_{12}E_{22}}{1-\mu_{12}\mu_{21}},\\
&Q_{22}=\frac{E_{22}}{1-\mu_{12}\mu_{21}},\quad Q_{66}=G_{12}
\end{aligned} \tag{18}$$

Considered shell model contains stresses which result in below forces and moments via integrating Eq. (16) over the thickness

$$\begin{Bmatrix}N_{\xi_1}\\ N_{\xi_2}\\ N_{\xi_1\xi_2}\end{Bmatrix}=\begin{pmatrix}E_{11} & E_{12} & E_{16}\\ E_{12} & E_{22} & E_{26}\\ E_{16} & E_{26} & E_{66}\end{pmatrix}\begin{Bmatrix}\varepsilon^0_{\xi_1}\\ \varepsilon^0_{\xi_2}\\ \gamma^0_{\xi_1\xi_2}\end{Bmatrix}-\begin{pmatrix}F_{11} & F_{12} & F_{16}\\ F_{12} & F_{22} & F_{26}\\ F_{16} & F_{26} & F_{66}\end{pmatrix}\begin{Bmatrix}\chi_{\xi_1}\\ \chi_{\xi_2}\\ 2\chi_{\xi_1\xi_2}\end{Bmatrix} \tag{19}$$

$$\begin{Bmatrix}M_{\xi_1}\\ M_{\xi_2}\\ M_{\xi_1\xi_2}\end{Bmatrix}=\begin{pmatrix}F_{11} & F_{12} & F_{16}\\ F_{12} & F_{22} & F_{26}\\ F_{16} & F_{26} & F_{66}\end{pmatrix}\begin{Bmatrix}\varepsilon^0_{\xi_1}\\ \varepsilon^0_{\xi_2}\\ \gamma^0_{\xi_1\xi_2}\end{Bmatrix}-\begin{pmatrix}H_{11} & H_{12} & H_{16}\\ H_{12} & H_{22} & H_{26}\\ H_{16} & H_{26} & H_{66}\end{pmatrix}\begin{Bmatrix}\chi_{\xi_1}\\ \chi_{\xi_2}\\ 2\chi_{\xi_1\xi_2}\end{Bmatrix} \tag{20}$$

in which

$$\begin{aligned}
&E_k=\int_{-h/2}^{h/2}\tilde{C}_k dz,\\
&F_k=\int_{-h/2}^{h/2}\tilde{C}_k z dz,\\
&H_k=\int_{-h/2}^{h/2}\tilde{C}_k z^2 dz,\\
&k=\{11,12,22,16,26,66\}
\end{aligned} \tag{21}$$

Represented in the below equations are the governing equations of conical shells based upon classical shell theory in terms of defined forces and moments as

$$\xi_1\frac{\partial N_{\xi_1}}{\partial \xi_1}+\frac{1}{\sin\beta}\frac{\partial N_{\xi_1\xi_2}}{\partial \xi_2}+N_{\xi_1}-N_{\xi_2}=I_0\frac{\partial^2 u}{\partial t^2} \tag{22}$$

$$\xi_1\frac{\partial N_{\xi_1\xi_2}}{\partial \xi_1}+\frac{1}{\sin\beta}\frac{\partial N_{\xi_2}}{\partial \xi_2}+2N_{\xi_1\xi_2}=I_0\frac{\partial^2 v}{\partial t^2} \tag{23}$$

$$\begin{aligned}&\xi_1\frac{\partial^2 M_{\xi_1}}{\partial \xi_1^{\,2}}+2\frac{\partial M_{\xi_1}}{\partial \xi_1}+\frac{2}{\sin\beta}\left(\frac{\partial^2 M_{\xi_1\xi_2}}{\partial \xi_1\partial \xi_2}+\frac{1}{\xi_1}\frac{\partial M_{\xi_1\xi_2}}{\partial \xi_2}\right)\\&+\frac{1}{\xi_1\sin^2\beta}\frac{\partial^2 M_\theta}{\partial \xi_2^{\,2}}-\frac{\partial M_{\xi_2}}{\partial \xi_1}-N_{\xi_2}\cot\beta\\&+\frac{\partial}{\partial \xi_1}\left(\xi_1 N_{\xi_1}\frac{\partial w}{\partial \xi_1}+\frac{1}{\sin\beta}N_{\xi_1\xi_2}\frac{\partial w}{\partial \xi_2}\right)\\&+\frac{1}{\sin\beta}\frac{\partial}{\partial \xi_2}\left(N_{\xi_1\xi_2}\frac{\partial w}{\partial \xi_1}+\frac{1}{\xi_1\sin\beta}N_{\xi_2}\frac{\partial w}{\partial \xi_2}\right)\\&=I_0\frac{\partial^2 w}{\partial t^2}+f(t)\end{aligned} \tag{24}$$

where $f(t)=F\cos(\omega t)$ and $I_0=\int_{-h/2}^{h/2}\rho dz$ is mass inertia. Note that F is force amplitude and ω is excitation frequency In order to simplify the governing equations and representing them with respect to strain components, Eqs. (19) and (20) should be placed into Eqs. (22) and (24) which gives

$$\begin{aligned}&\xi_1\frac{\partial}{\partial \xi_1}[E_{11}\varepsilon_{\xi_1}^0+E_{12}\varepsilon_{\xi_2}^0+E_{16}\gamma_{\xi_1\xi_2}^0-F_{11}\chi_{\xi_1}\\&-F_{21}\chi_{\xi_2}-2F_{16}\chi_{\xi_1\xi_2}]+\frac{1}{\sin\beta}\frac{\partial}{\partial \xi_2}[E_{16}\varepsilon_{\xi_1}^0\\&+E_{26}\varepsilon_{\xi_2}^0+E_{66}\gamma_{\xi_1\xi_2}^0-F_{16}\chi_{\xi_1}-F_{26}\chi_{\xi_2}\\&-2F_{66}\chi_{\xi_1\xi_2}]+E_{11}\varepsilon_{\xi_1}^0+E_{12}\varepsilon_{\xi_2}^0+E_{16}\gamma_{\xi_1\xi_2}^0\\&-F_{11}\chi_{\xi_1}-F_{21}\chi_{\xi_2}-2F_{16}\chi_{\xi_1\xi_2}-(E_{12}\varepsilon_{\xi_1}^0\\&+E_{22}\varepsilon_{\xi_2}^0+E_{26}\gamma_{\xi_1\xi_2}^0-F_{12}\chi_{\xi_1}-F_{22}\chi_{\xi_2}\\&-2F_{26}\chi_{\xi_1\xi_2})=I_0\frac{\partial^2 u}{\partial t^2}\end{aligned} \tag{25}$$

$$\begin{aligned}&\xi_1\frac{\partial}{\partial \xi_1}[E_{16}\varepsilon_{\xi_1}^0+E_{26}\varepsilon_{\xi_2}^0+E_{66}\gamma_{\xi_1\xi_2}^0\\&-F_{16}\chi_{\xi_1}-F_{26}\chi_{\xi_2}-2F_{66}\chi_{\xi_1\xi_2}]\\&+\frac{1}{\sin\beta}\frac{\partial}{\partial \xi_2}[E_{12}\varepsilon_{\xi_1}^0+E_{22}\varepsilon_{\xi_2}^0+E_{26}\gamma_{\xi_1\xi_2}^0\\&-F_{12}\chi_{\xi_1}-F_{22}\chi_{\xi_2}-2F_{26}\chi_{\xi_1\xi_2}]\\&+2[E_{16}\varepsilon_{\xi_1}^0+E_{26}\varepsilon_{\xi_2}^0+E_{66}\gamma_{\xi_1\xi_2}^0\\&-F_{16}\chi_{\xi_1}-F_{26}\chi_{\xi_2}-2F_{66}\chi_{\xi_1\xi_2}]=I_0\frac{\partial^2 v}{\partial t^2}\end{aligned} \tag{26}$$

$$\begin{aligned}&(\xi_1\frac{\partial^2}{\partial \xi_1^{\,2}}+2\frac{\partial}{\partial \xi_1})[F_{11}\varepsilon_{\xi_1}^0+F_{12}\varepsilon_{\xi_2}^0+F_{16}\gamma_{\xi_1\xi_2}^0\\&-H_{11}\chi_{\xi_1}-H_{21}\chi_{\xi_2}-2H_{16}\chi_{\xi_1\xi_2}]\\&+\frac{2}{\sin\beta}(\frac{\partial^2}{\partial \xi_1\partial \xi_2}+\frac{1}{\xi_1}\frac{\partial}{\partial \xi_2})[F_{16}\varepsilon_{\xi_1}^0+F_{26}\varepsilon_{\xi_2}^0\\&+F_{66}\gamma_{\xi_1\xi_2}^0-H_{16}\chi_{\xi_1}-H_{26}\chi_{\xi_2}-2H_{66}\chi_{\xi_1\xi_2}]\\&+(\frac{1}{\xi_1\sin^2\beta}\frac{\partial^2}{\partial \xi_2^{\,2}}-\frac{\partial}{\partial \xi_1})[F_{12}\varepsilon_{\xi_1}^0+F_{22}\varepsilon_{\xi_2}^0\\&+F_{26}\gamma_{\xi_1\xi_2}^0-H_{12}\chi_{\xi_1}-H_{22}\chi_{\xi_2}-2H_{26}\chi_{\xi_1\xi_2}]\\&-[E_{12}\varepsilon_{\xi_1}^0+E_{22}\varepsilon_{\xi_2}^0+E_{26}\gamma_{\xi_1\xi_2}^0-F_{12}\chi_{\xi_1}\\&-F_{22}\chi_{\xi_2}-2F_{26}\chi_{\xi_1\xi_2}]\cot\beta\\&+\frac{\partial}{\partial \xi_1}(\xi_1[E_{11}\varepsilon_{\xi_1}^0+E_{12}\varepsilon_{\xi_2}^0+E_{16}\gamma_{\xi_1\xi_2}^0\\&-F_{11}\chi_{\xi_1}-F_{21}\chi_{\xi_2}-2F_{16}\chi_{\xi_1\xi_2}]\frac{\partial w}{\partial \xi_1}\\&+\frac{1}{\sin\beta}[E_{16}\varepsilon_{\xi_1}^0+E_{26}\varepsilon_{\xi_2}^0+E_{66}\gamma_{\xi_1\xi_2}^0\\&-F_{16}\chi_{\xi_1}-F_{26}\chi_{\xi_2}-2F_{66}\chi_{\xi_1\xi_2}]\frac{\partial w}{\partial \xi_2})\\&+\frac{1}{\sin\beta}\frac{\partial}{\partial \xi_2}([E_{16}\varepsilon_{\xi_1}^0+E_{26}\varepsilon_{\xi_2}^0+E_{66}\gamma_{\xi_1\xi_2}^0\\&-F_{16}\chi_{\xi_1}-F_{26}\chi_{\xi_2}-2F_{66}\chi_{\xi_1\xi_2}]\frac{\partial w}{\partial \xi_1}\\&+\frac{1}{\xi_1\sin\beta}[E_{12}\varepsilon_{\xi_1}^0+E_{22}\varepsilon_{\xi_2}^0+E_{26}\gamma_{\xi_1\xi_2}^0\\&-F_{12}\chi_{\xi_1}-F_{22}\chi_{\xi_2}-2F_{26}\chi_{\xi_1\xi_2}]\frac{\partial w}{\partial \xi_2})=I_0\frac{\partial^2 w}{\partial t^2}\end{aligned} \tag{27}$$

4. Solution procedure

Herein, the solution of nonlinear governing equations of multi-scale conical shells and annular sector plates has been presented. Firstly, it should be noted that the edges of the structure are simply-supported based upon following conditions

$$\begin{aligned}&w=v=M_{\xi_1}=N_{\xi_1\xi_2}=0 \ \text{ at } \xi_1=\xi_0,\xi_0+L\\&w=u=M_{\xi_2}=N_{\xi_1\xi_2}=0 \ \text{ at } \xi_2=0,\psi\end{aligned} \tag{28}$$

According to the thin shell and sector plate formulation, the displacement field may be selected as

$$u=\sum_{i=1}^{\infty}\sum_{j=1}^{\infty}U_{ij}(t)\frac{\partial H_i(\xi_1)}{\partial \xi_1}R_j(\xi_2) \tag{29}$$

$$v=\sum_{i=1}^{\infty}\sum_{j=1}^{\infty}V_{ij}(t)H_i(\xi_1)\frac{\partial R_j(\xi_2)}{\partial \xi_2} \tag{30}$$

$$w=\sum_{i=1}^{\infty}\sum_{j=1}^{\infty}W_{ij}(t)H_i(\xi_1)R_j(\xi_2) \tag{31}$$

where (U ,V ,W) are the displacements amplitudes and the functions H_i and R_j are the test functions which are selected as

$$H_i(\xi_1)=\sin\frac{i\pi(\xi_1-\xi_0)}{L},\quad R_j(\xi_2)=\sin\left(\frac{j\pi\xi_2}{\psi}\right) \tag{32}$$

Arranging the governing equations as Y_i (u, v, w)=0 with (i=1,2,3) and inserting field components presented as Eqs.(29)-(31) into Y_i yields following equations with the use of Galerkin's technique

$$\int_{\xi_0}^{\xi_0+L}\int_0^{\psi} Y_1\frac{\partial H_i(\xi_1)}{\partial\xi_1}R_j(\xi_2)\xi_1\sin\beta d\xi_1 d\xi_2=0 \tag{33}$$

$$\int_{\xi_0}^{\xi_0+L}\int_0^{\psi} Y_2 H_i(\xi_1)\frac{\partial R_j(\xi_2)}{\partial\xi_2}\xi_1\sin\beta d\xi_1 d\xi_2=0 \tag{34}$$

$$\int_{\xi_0}^{\xi_0+L}\int_0^{\psi} Y_3 H_i(\xi_1)R_j(\xi_2)\xi_1\sin\beta d\xi_1 d\xi_2=0 \tag{35}$$

After solving Eqs. (33)-(35) by neglecting in-plane inertias, three governing equations will be derived

$$\Phi_{11}U+\Phi_{21}V+\Phi_{31}W+G_1W^2=0 \tag{36}$$

$$\Phi_{12}U+\Phi_{22}V+\Phi_{32}W+G_2W^2=0 \tag{37}$$

$$\Phi_{13}U+\Phi_{23}V+\Phi_{33}W+G_3W^2+G_4W^3+n_1UW+n_2VW+M\ddot{W}=F\cos(\omega t) \tag{38}$$

in which Φ_{ij} are stiffness matrix components; M is mass matrix and G_i are nonlinear stiffness matrices. With the use of Eqs. (36) and (37), U and V are calculated as

$$U=\frac{\Phi_{21}\Phi_{32}-\Phi_{22}\Phi_{31}}{\Phi_{11}\Phi_{22}-\Phi_{12}\Phi_{21}}W+\frac{G_2\Phi_{21}-G_1\Phi_{22}}{\Phi_{11}\Phi_{22}-\Phi_{12}\Phi_{21}}W^2$$
$$V=\frac{\Phi_{12}\Phi_{31}-\Phi_{11}\Phi_{32}}{\Phi_{11}\Phi_{22}-\Phi_{12}\Phi_{21}}W+\frac{G_1\Phi_{12}-G_2\Phi_{11}}{\Phi_{11}\Phi_{22}-\Phi_{12}\Phi_{21}}W^2 \tag{39}$$

Therefore, Eq. (38), with the aid of Eq. (39) can be reduced to below equation

$$\ddot{W}+\frac{T_1}{M}W+\frac{T_2}{M}W|W|+\frac{T_3}{M}W^3=\frac{F}{M}\cos(\omega t) \tag{40}$$

for which

$$T_1=K_{13}\frac{K_{21}K_{32}-K_{22}K_{31}}{K_{11}K_{22}-K_{12}K_{21}}+K_{33}+K_{23}\frac{K_{12}K_{31}-K_{11}K_{32}}{K_{11}K_{22}-K_{12}K_{21}}$$
$$T_2=+G_3+K_{13}\frac{G_2K_{21}-G_1K_{22}}{K_{11}K_{22}-K_{12}K_{21}}+K_{23}\frac{G_1K_{12}-G_2K_{11}}{K_{11}K_{22}-K_{12}K_{21}}+n_1\frac{K_{21}K_{32}-K_{22}K_{31}}{K_{11}K_{22}-K_{12}K_{21}}+n_2\frac{K_{12}K_{31}-K_{11}K_{32}}{K_{11}K_{22}-K_{12}K_{21}}$$
$$T_3=+G_4+n_1\frac{G_2K_{21}-G_1K_{22}}{K_{11}K_{22}-K_{12}K_{21}}+n_2\frac{G_1K_{12}-G_2K_{11}}{K_{11}K_{22}-K_{12}K_{21}} \tag{41}$$

Exact solution of above equation can be introduced based on Jacobi elliptic function (cn) as (Feng and Meng 2017)

$$W=\tilde{W}cn(\vartheta t,k^2) \tag{42}$$

Note that k^2 is the modulus of the elliptic function; $\tilde{W}$ is vibration amplitude. It should be pointed out that ϑ is the frequency of elliptic function. Based on the Fourier expansion, the Jacobi elliptic function (cn) can be expressed as a series of corresponding trigonometric function as

$$cn(\vartheta t,k^2)=\frac{2\pi}{kK}\sum_{r=0}^{\infty}\frac{q^{r+\frac{1}{2}}}{1+q^{2r+1}}\cos\left((2r+1)\frac{\pi\vartheta t}{2K}\right) \tag{43}$$

where K(k) is the complete elliptic integral of the first kind; $q=\exp(-\pi K'/K)$ and $K'=K(l)$ is the associated complete elliptic integral of the first kind. Also, the elliptic modulus can be defines as

$$k^2=\frac{\frac{T_2}{M}|\tilde{W}|a_1+\frac{T_3}{M}\tilde{W}^2}{2\left(\frac{T_1}{M}+\frac{T_2}{M}|\tilde{W}|(a_0+a_1)+\frac{T_3}{M}\tilde{W}^2\right)} \tag{44}$$

where a_0 and a_1 are two constants. The vibration frequency depends on the period of elliptic function, $\Upsilon=2\pi/T$ in which

$$T=\frac{4K(k)}{\vartheta} \tag{45}$$

where

$$K=\int_0^{\pi/2}\frac{d\theta}{\sqrt{1-k^2\sin^2\theta}} \tag{46}$$

However, Eq. (42) must be inserted into Eq. (4) to derive amplitude-frequency curves as explained by Mirjavadi *et al*. (2020). Also, some normalized parameters can be introduced in this paper such as

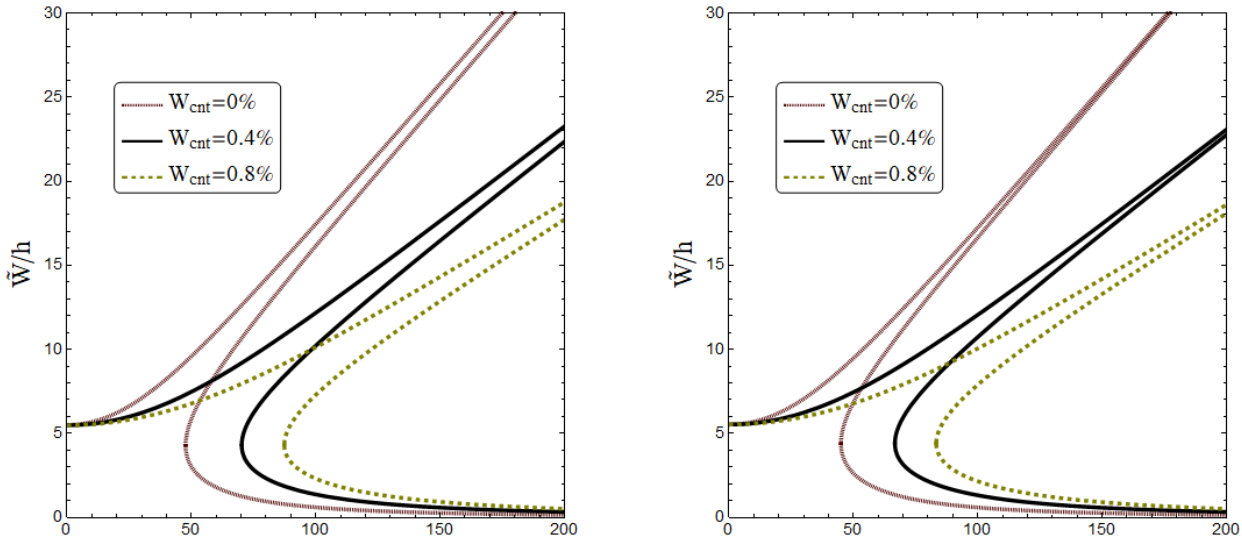

(a) truncated conical shell (b) annular plate

Fig. 4 Forced vibration curves of multi-scale conical shells and annular plates for various CNT weight fraction (V_f=0, $\tilde{F}$=0.001, α=50)

$$\Omega = \Upsilon L^2 \sqrt{\frac{\rho_m}{E_m h^2}}\ , \tilde{F} = F\frac{h^2}{A_{11}} \tag{48}$$

5. Results and discussions

Presented in this section is nonlinear forced vibration characteristics of multi-scale epoxy/CNT/fiberglass truncated conical shells and annular plates subjected to transverse harmonic load. In previous sections, a Mori-Tanaka model was employed for evaluating multi-scale material properties. Also, Jacobi elliptic functions were used for solving the governing equations and deriving forced vibration curves of the multi-scale annular plate and conical shell. This section provides new findings for demonstrating the significance of CNT distribution, geometric nonlinearity, applied force, fiberglass volume, open angle and fiber directions on forced vibration characteristics of multi-scale annular plates and truncated conical shells.

Based on various values of inner to outer radius ratio (r_0/r_1) of nano-composite annular plate, Table 2 presents the validation of vibration frequency with that of Liu *et al.* (2019). In this table it is assumed that r_0/r_1=0.1, 0.2 and 0.3 and plate thickness is h/r_1=0.05. Also, uniform dispersion of carbon-based inclusion within the matrix is assumed. One can see the excellent agreement among obtained frequencies and the results provided by Liu *et al.* (2019).

For both multi-scale truncated conical shell and annular plate, forced vibration curves based on various CNT weight fraction (W_{cnt}) are shown in Fig. 4 when the open angle is considered as $\psi=2\pi$. Also, the normalized value of applied for is considered as $\tilde{F}$=0.001. This figure shows the normalized deflection ($\tilde{W}/h$) variation of truncated conical shell and annular plate with excitation frequency. It is obvious that deflection value is increasing with respect to excitation frequency and resonance occurs at a particular value of excitation frequency. It is also seen that frequency-amplitude curves of truncated conical shell and annular plate moves to the right by increase of CNT weight fraction. This means that resonance occurs at higher values of excitation frequency when the CNT weight fraction increases. So, adding CNT into the matrix will improve forced vibration characteristics of the truncated conical shells and annular plates.

Based on various values of fiberglass volume (V_f), Fig. 5 illustrates the variation of frequency-deflection curves of truncated conical shell and annular plate. The weight fraction of CNTs is chosen to be W_{cnt}=0.2%. Truncated distance is considered as ξ_0=0.4L. This figure indicates that higher values for fiberglass volume result in greater excitation frequencies due to increased stiffness of the shell and annular plate. Therefore, it can be concluded that both fiberglass and CNT content can affect forced vibration behavior of annular plates and truncated conical shells.

Forced vibration curves of multi-scale annular sectors and truncated conical segments for various open angles are plotted in Fig. 6 by assuming that W_{cnt}=0.2% and V_f=0.1. Annular sectors and truncated conical segments with different values of open angle have diverse nonlinear vibration behaviors. Actually, annular sectors and truncated conical segments with lower open angle has more deviation to the right due to increase of nonlinear effects. Thus, as the open angle increases the nonlinear effects become less prominent and frequency-amplitude curves have less deviations. In this figure, the most notable influence of nonlinearity is obtained when ψ=30 degree.

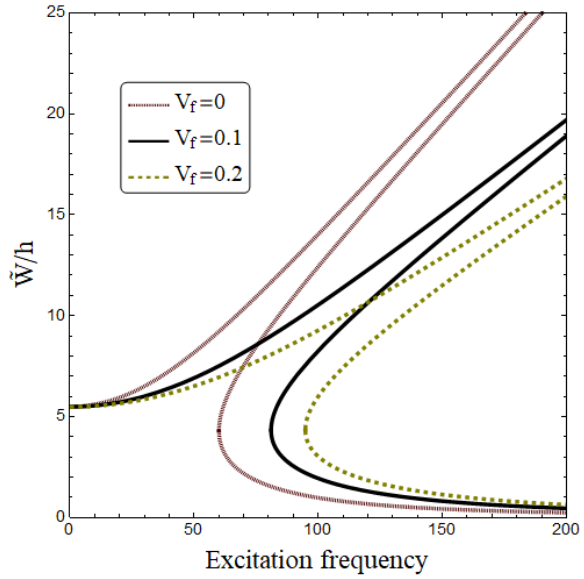

(a) truncated conical shell

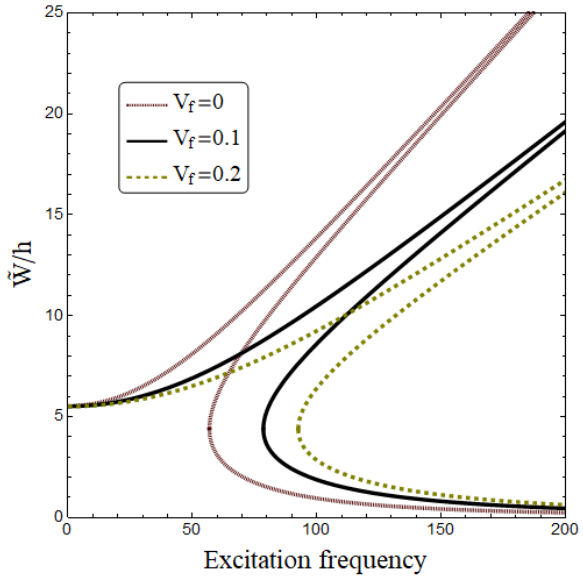

(b) annular plate

Fig. 5 Forced vibration curves of multi-scale conical shells and annular plates for various fiber volume fraction (W_{cnt}=0.2%, $\tilde{F}$=0.001, α=50)

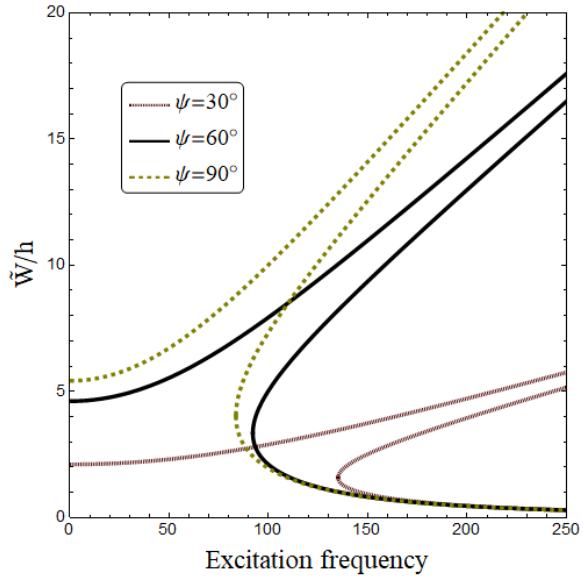

(a) truncated conical shell segment

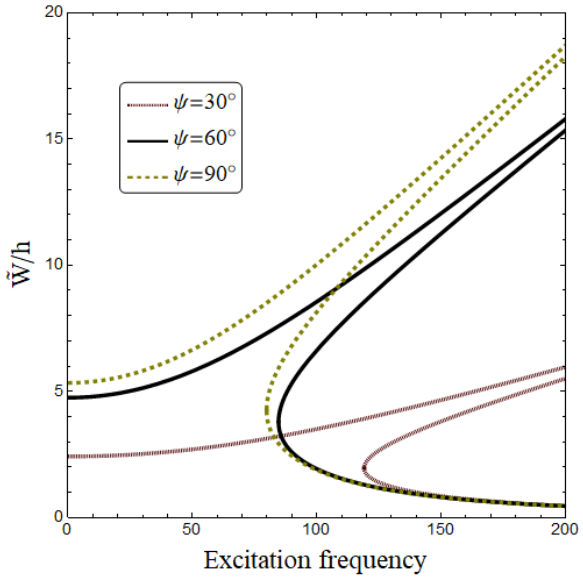

(b) annular plate sector

Fig. 6 Forced vibration curves of multi-scale conical shell segments and annular plate sector for various opening angles (V_f=0.1, W_{cnt}=0.2%, $\tilde{F}$=0.001, α=50)

Based on various values of fiber orientation (θ), Fig. 7 depicts the variation of normalized deflection of annular sector with respect to excitation frequency. It is assumed that W_{cnt}=0.2% and V_f=0.1. It must be pointed out that θ=0 results in fiber direction parallel to ξ_1 axis. One can see that increasing in orientation angle yields lower excitation frequency. Accordingly, as the value of fiber orientation is greater, the structural stiffness of annular plate is decreased. Hence, the forced vibration behaviors of annular plates made of multi-scale composites rely on the orientations of included fibers.

In Fig. 8, the variation of normalized deflection of annular sector with respect to excitation frequency is plotted according to diverse values for normalized force amplitude $\tilde{F}$. It is clear that force amplitude has no impact on the magnitude of excitation frequency, but it greatly affects the values of deflections. Indeed, higher values for normalized force amplitude yield larger deflections, but un-varied resonance frequency location. So, in nonlinear analysis of forced vibrations of annular plates, the magnitude of force amplitude has a key load in determining the response branches.

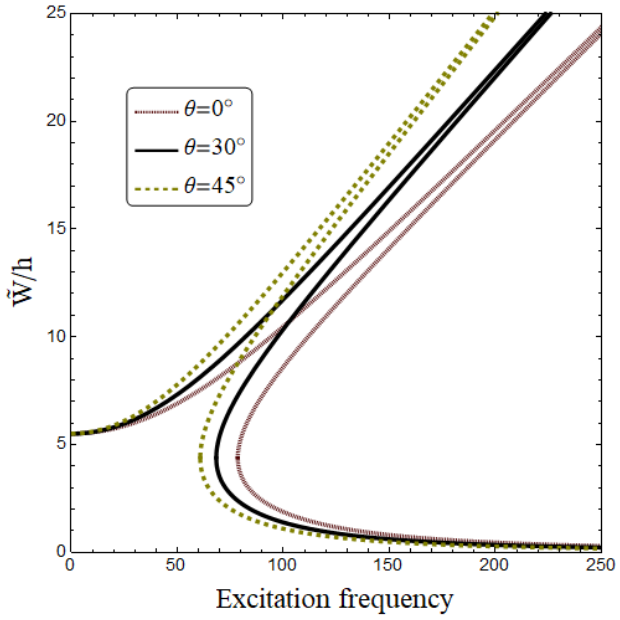

Fig. 7 Forced vibration curves of multi-scale annular sector for various fiber angles (W_{cnt}=0.2%, V_f=0.1)

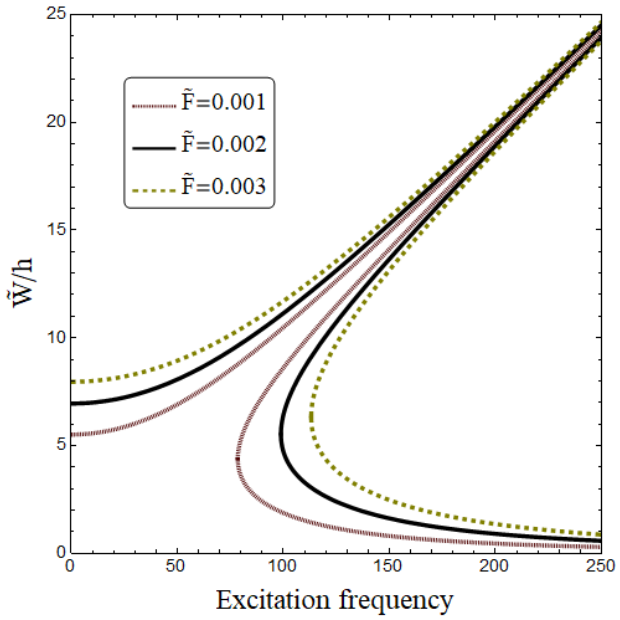

Fig. 8 Forced vibration curves of multi-scale annular sector for various force amplitude (W_{cnt}=0.2%, V_f=0.1)

Fig.9 depicts forced vibration properties of multi-scale annular plates affected by diverse values of truncated distance (ξ_0) at fixed values of W_{cnt}=0.2%, V_f=0.1, and $\psi=2\pi$. Truncated distance of the plate has great influences on deviation of frequency-amplitude curves. Actually, more deviation is observed for higher values of truncated distance which means that nonlinear effects are more announced. So, the geometry of annular plate is very important for determining the forced vibration properties.

6. Conclusions

Based on an analytical trend, the presented article examined nonlinear forced vibrations of truncated conical shells and annular plates made of multi-scale materials. The multi-scale composite is consist of epoxy, random CNTs and glass fibers which were included into the calculations based on Mori-Tanaka scheme. Jacobi elliptic functions were employed for determining the frequency-amplitude curves. In the below statements, new findings are introduced:

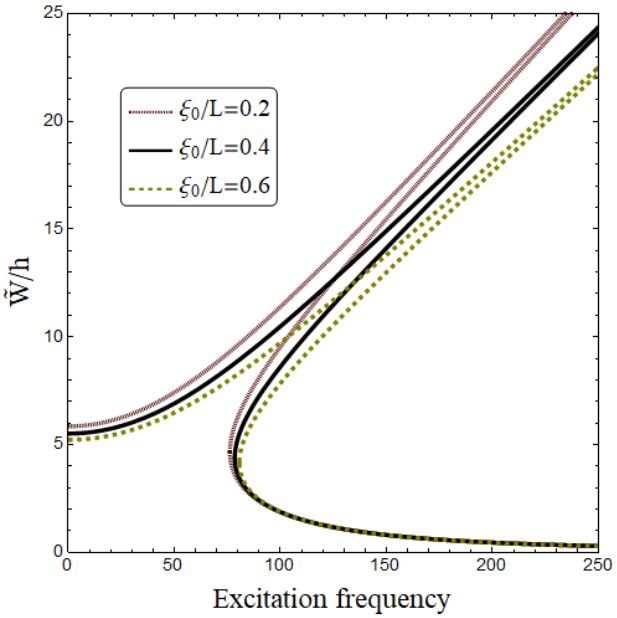

Fig. 9 Forced vibration curves of multi-scale annular sector for various sector radius (W_{cnt}=0.2%, V_f=0.1)

- The resonance occurs at higher values of excitation frequency when the CNT weight fraction increases.
- Higher values for fiberglass volume result in greater excitation frequencies due to increased stiffness of the annular sector.
- As the open angle increases the nonlinear effects become less prominent and frequency-amplitude curves have less deviations.
- Increasing in fiber orientation angle yields lower excitation frequency.
- Nonlinear effects become less prominent as the value of truncated distance declines.

Acknowledgements

The first and second authors would like to thank FPQ (Fidar project Qaem) for providing the fruitful and useful help.

References

Abualnour, M., Chikh, A., Hebali, H., Kaci, A., Tounsi, A., Bousahla, A.A. and Tounsi, A. (2019), "Thermomechanical analysis of antisymmetric laminated reinforced composite plates using a new four variable trigonometric refined plate theory. *Comput. Concrete*, **24**(6), 489-498. https://doi.org/10.12989/cac.2019.24.6.489.

Addou, F.Y., Meradjah, M., Bousahla, A.A., Benachour, A., Bourada, F., Tounsi, A. and Mahmoud, S.R. (2019), "Influences of porosity on dynamic response of FG plates resting on Winkler/Pasternak/Kerr foundation using quasi 3D HSDT. *Comput. Concrete*, **24**(4), 347-367. https://doi.org/10.12989/cac.2019.24.4.347.

Ahmed, R.A., Fenjan, R.M. and Faleh, N.M. (2019), "Analyzing post-buckling behavior of continuously graded FG nanobeams with geometrical imperfections," *Geomech. Eng.*, **17**(2), 175-180. https://doi.org/10.12989/gae.2019.17.2.175.

Azimi, M., Mirjavadi, S.S., Shafiei, N. and Hamouda, A.M.S. (2017), "Thermo-mechanical vibration of rotating axially functionally graded nonlocal Timoshenko beam", *Appl. Phys. A*, **123**(1), 104.

Azimi, M., Mirjavadi, S.S., Shafiei, N., Hamouda, A.M.S. and Davari, E. (2018), "Vibration of rotating functionally graded Timoshenko nano-beams with nonlinear thermal distribution", *Mech. Adv. Mater. Struct*, **25**(6), 467-480.

Barati, M.R. and Zenkour, A.M. (2017), "Post-buckling analysis of refined shear deformable graphene platelet reinforced beams with porosities and geometrical imperfection", *Compos. Struct.*, **181**, 194-202. https://doi.org/10.1016/j.compstruct.2017.08.082.

Balubaid, M., Tounsi, A., Dakhel, B. and Mahmoud, S.R. (2019), "Free vibration investigation of FG nanoscale plate using nonlocal two variables integral refined plate theory", *Comput. Concrete*, **24**(6), 579-586. https://doi.org/10.12989/cac.2019.24.6.579.

Batou, B., Nebab, M., Bennai, R., Atmane, H.A., Tounsi, A. and Bouremana, M. (2019), "Wave dispersion properties in imperfect sigmoid plates using various HSDTs", *Steel Compos. Struct.*, **33**(5), 699-716. https://doi.org/10.12989/scs.2019.33.5.699.

Bellal, M., Hebali, H., Heireche, H., Bousahla, A.A., Tounsi, A., Bourada, F. and Tounsi, A. (2020), "Buckling behavior of a single-layered graphene sheet resting on viscoelastic medium via nonlocal four-unknown integral model", *Steel Compos. Struct.*, **34**(5), 643-655. https://doi.org/10.12989/scs.2020.34.5.643.

Berghouti, H., Adda Bedia, E.A., Benkhedda, A. and Tounsi, A. (2019), "Vibration analysis of nonlocal porous nanobeams made of functionally graded material", *Adv. Nano Res.*, 7(5), 351-364. https://doi.org/10.12989/anr.2019.7.5.351.

Bouamoud, A., Boucham, B., Bourada, F., Houari, M.S.A. and Tounsi, A. (2019), "Thermomechanical bending investigation of FGM sandwich plates using four shear deformation plate theory", *Steel Compos. Struct.*, **32**(5), 611-632. https://doi.org/10.12989/scs.2019.32.5.611.

Bourada, F., Bousahla, A.A., Bourada, M., Azzaz, A., Zinata, A.

and Tounsi, A. (2019), "Dynamic investigation of porous functionally graded beam using a sinusoidal shear deformation theory", *Wind Struct.*, **28**(1), 19-30. https://doi.org/10.12989/was.2019.28.1.019.

Boussoula, A., Boucham, B., Bourada, M., Bourada, F., Tounsi, A., Bousahla, A.A. and Tounsi, A. (2020), "A simple nth-order shear deformation theory for thermomechanical bending analysis of different configurations of FG sandwich plates", *Smart Struct. Syst.*, **25**(2), 197-218. https://doi.org/10.12989/sss.2020.25.2.197.

Boutaleb, S., Benrahou, K. H., Bakora, A., Algarni, A., Bousahla, A.A., Tounsi, A. and Mahmoud, S.R. (2019), "Dynamic analysis of nanosize FG rectangular plates based on simple nonlocal quasi 3D HSDT", *Adv. Nano Res.*, **7**(3), 191-208. https://doi.org/10.12989/anr.2019.7.3.191.

Chaabane, L.A., Bourada, F., Sekkal, M., Zerouati, S., Zaoui, F.Z., Tounsi, A. and Tounsi, A. (2019), "Analytical study of bending and free vibration responses of functionally graded beams resting on elastic foundation", *Struct. Eng. Mech.*, **71**(2), 185-196. https://doi.org/10.12989/sem.2019.71.2.185.

Draiche, K., Bousahla, A.A., Tounsi, A., Alwabli, A.S., Tounsi, A. and Mahmoud, S.R. (2019), "Static analysis of laminated reinforced composite plates using a simple first-order shear deformation theory", *Comput. Concrete*, **24**(4), 369-378. https://doi.org/10.12989/cac.2019.24.4.369.

Draoui, A., Zidour, M., Tounsi, A. and Adim, B. (2019), "Static and dynamic behavior of nanotubes-reinforced sandwich plates using (FSDT)", *J. Nano Res.*, **57**, 117-135. https://doi.org/10.4028/www.scientific.net/JNanoR.57.117.

Dai, T., Yang, Y., Dai, H.L., Tang, H. and Lin, Z.Y. (2019), "Hygrothermal mechanical behaviors of a porous FG-CRC annular plate with variable thickness considering aggregation of CNTs", *Compos. Struct.*, **215**, 198-213. https://doi.org/10.1016/j.compstruct.2019.02.061.

Dong, Y.H., Li, Y.H., Chen, D. and Yang, J. (2018), "Vibration characteristics of functionally graded graphene reinforced porous nanocomposite cylindrical shells with spinning motion", *Compos. Part B: Eng.*, **145**, 1-13.

Feng, C., Kitipornchai, S. and Yang, J. (2017), "Nonlinear bending of polymer nanocomposite beams reinforced with non-uniformly distributed graphene platelets (GPLs)", *Compos. Part B: Eng.*, **110**, 132-140.

Feng, Q. and Meng, F. (2017), "Traveling wave solutions for fractional partial differential equations arising in mathematical physics by an improved fractional Jacobi elliptic equation method", *Math. Method. Appl. Sci.*, **40**(10), 3676-3686. https://doi.org/10.1002/mma.4254.

Hellal, H., Bourada, M., Hebali, H., Bourada, F., Tounsi, A., Bousahla, A.A. and Mahmoud, S.R. (2019), "Dynamic and stability analysis of functionally graded material sandwich plates in hygro-thermal environment using a simple higher shear deformation theory", *J. Sandw. Struct. Mater.*, 1099636219845841.https://doi.org/10.1177%2F1099636219845841.

Hussain, M., Naeem, M.N., Tounsi, A. and Taj, M. (2019), "Nonlocal effect on the vibration of armchair and zigzag SWCNTs with bending rigidity", *Adv. Nano Res.*, **7**(6), 431-442. https://doi.org/10.12989/anr.2019.7.6.431.

Houari, T., Bessaim, A., Houari, M.S.A., Benguediab, M. and Tounsi, A. (2018), "Bending analysis of advanced composite plates using a new quasi 3D plate theory", *Steel Compos. Struct.*, **26**(5), 557-572. https://doi.org/10.12989/scs.2018.26.5.557.

Kaddari, M., Kaci, A., Bousahla, A.A., Tounsi, A., Bourada, F., Bedia, E.A. and Al-Osta, M.A. (2020), "A study on the structural behaviour of functionally graded porous plates on elastic foundation using a new quasi-3D model: bending and free vibration analysis", *Comput. Concrete*, **25**(1), 37. https://doi.org/10.12989/cac.2020.25.1.037.

Khiloun, M., Bousahla, A.A., Kaci, A., Bessaim, A., Tounsi, A. and Mahmoud, S.R. (2019), "Analytical modeling of bending and vibration of thick advanced composite plates using a four-variable quasi 3D HSDT", *Eng. with Comput.*, 1-15. https://doi.org/10.1007/s00366-019-00732-1.

Kazakov, I.A., Krasnovskii, A.N. and Kishuk, P.S. (2019), "The influence of randomly oriented CNTs on the elastic properties of unidirectionally aligned composites", *Mech. Mater.*, **134**, 54-60. https://doi.org/10.1016/j.mechmat.2019.04.002.

Keleshteri, M.M., Asadi, H. and Aghdam, M.M. (2019), "Nonlinear bending analysis of FG-CNTRC annular plates with variable thickness on elastic foundation", *Thin-Wall. Struct.*, **135**, 453-462. https://doi.org/10.1016/j.tws.2018.11.020.

Liu, D., Li, Z., Kitipornchai, S. and Yang, J. (2019), "Three-dimensional free vibration and bending analyses of functionally graded graphene nanoplatelets-reinforced nanocomposite annular plates", *Compos. Struct.*, **229**, 111453. https://doi.org/10.1016/j.compstruct.2019.111453.

Medani, M., Benahmed, A., Zidour, M., Heireche, H., Tounsi, A., Bousahla, A.A. and Mahmoud, S.R. (2019), "Static and dynamic behavior of (FG-CNT) reinforced porous sandwich plate using energy principle", *Steel Compos. Struct.*, **32**(5), 595-610. https://doi.org/10.12989/scs.2019.32.5.595.

Meksi, R., Benyoucef, S., Mahmoudi, A., Tounsi, A., Adda Bedia, E.A. and Mahmoud, S.R. (2019), "An analytical solution for bending, buckling and vibration responses of FGM sandwich plates", *J. Sandw. Struct. Mater.*, **21**(2), 727-757. https://doi.org/10.1177%2F1099636217698443.

Marynowski, K. (2017), Free vibration analysis of an axially moving multiscale composite plate including thermal effect", *Int. J. Mech. Sci.*, **120**, 62-69. https://doi.org/10.1016/j.ijmecsci.2016.11.013.

Mirjavadi, S.S., Rabby, S., Shafiei, N., Afshari, B.M. and Kazemi, M. (2017), "On size-dependent free vibration and thermal buckling of axially functionally graded nanobeams in thermal environment", *Appl. Phys. A*, **123**(5), 315.

Mirjavadi, S.S., Afshari, B.M., Shafiei, N., Hamouda, A.M.S. and Kazemi, M. (2017), "Thermal vibration of two-dimensional functionally graded (2D-FG) porous Timoshenko nanobeams. *Steel Compos. Struct.*, **25**(4), 415-426. https://doi.org/10.12989/scs.2017.25.4.415.

Mirjavadi, S.S., Afshari, B.M., Barati, M.R. and Hamouda, A.M.S. (2018), "Strain gradient based dynamic response analysis of heterogeneous cylindrical microshells with porosities under a moving load", *Mater. Res. Express*, **6**(3), 035029.

Mirjavadi, S.S., Afshari, B.M., Khezel, M., Shafiei, N., Rabby, S. and Kordnejad, M. (2018), "Nonlinear vibration and buckling of functionally graded porous nanoscaled beams", *J. Brazilian Soc. Mech. Sci. Eng.*, **40**(7), 352.

Mirjavadi, S.S., Forsat, M., Hamouda, A.M.S. and Barati, M.R. (2019), "Dynamic response of functionally graded graphene nanoplatelet reinforced shells with porosity distributions under transverse dynamic loads", *Mater. Res. Express*, **6**(7), 075045.

Mirjavadi, S.S., Forsat, M., Nikookar, M., Barati, M.R. and Hamouda, A.M.S. (2019), "Nonlinear forced vibrations of sandwich smart nanobeams with two-phase piezo-magnetic face sheets", *The European Phys. J. Plus*, **134**(10), 508.

Mirjavadi, S.S., Afshari, B.M., Barati, M.R. and Hamouda, A.M.S. (2019), "Transient response of porous FG nanoplates subjected to various pulse loads based on nonlocal stress-strain gradient theory", *Eur. J. Mech.-A/Solids*, **74**, 210-220.

Mirjavadi, S.S., Afshari, B.M., Barati, M.R. and Hamouda, A.M.S. (2019), "Nonlinear free and forced vibrations of graphene nanoplatelet reinforced microbeams with geometrical imperfection", *Microsyst. Technologies*, **25**, 3137-3150.

Mirjavadi, S.S., Forsat, M., Barati, M.R., Abdella, G.M., Hamouda, A.M.S., Afshari, B.M. and Rabby, S. (2019), "Post-buckling analysis of piezo-magnetic nanobeams with geometrical imperfection and different piezoelectric contents", *Microsyst. Technologies*, **25**(9), 3477-3488.

Mirjavadi, S.S., Forsat, M., Barati, M.R., Abdella, G.M., Afshari, B.M., Hamouda, A.M.S. and Rabby, S. (2019), "Dynamic response of metal foam FG porous cylindrical micro-shells due to moving loads with strain gradient size-dependency," *The European Phys. J. Plus*, **134**(5), 214.

Mori, T. and Tanaka, K. (1973), "Average stress in matrix and average elastic energy of materials with misfitting inclusions", *Acta metallurgica*, **21**(5), 571-574. https://doi.org/10.1016/0001-6160(73)90064-3.

Rahmani, M.C., Kaci, A., Bousahla, A.A., Bourada, F., Tounsi, A., Bedia, E.A. and Tounsi, A. (2020), "Influence of boundary conditions on the bending and free vibration behavior of FGM sandwich plates using a four-unknown refined integral plate theory", *Comput. Concrete*, **25**(3), 225-244. https://doi.org/10.12989/cac.2020.25.3.225.

Refrafi, S., Bousahla, A.A., Bouhadra, A., Menasria, A., Bourada, F., Tounsi, A. and Tounsi, A. (2020), "Effects of hygro-thermo-mechanical conditions on the buckling of FG sandwich plates resting on elastic foundations", *Comput. Concrete*, **25(**4), 311-325. DOI: https://doi.org/10.12989/cac.2020.25.4.311.

Safaei, B., Moradi-Dastjerdi, R., Qin, Z. and Chu, F. (2019). Frequency-dependent forced vibration analysis of nanocomposite sandwich plate under thermo-mechanical loads", *Compos. Part B: Eng.*, **161**, 44-54.

Safarpour, M., Ghabussi, A., Ebrahimi, F., Habibi, M. and Safarpour, H. (2020), "Frequency characteristics of FG-GPLRC viscoelastic thick annular plate with the aid of GDQM", *Thin-Wall. Struct.*, **150**, 106683. https://doi.org/10.1016/j.tws.2020.106683.

Sahla, M., Saidi, H., Draiche, K., Bousahla, A.A., Bourada, F. and Tounsi, A. (2019), "Free vibration analysis of angle-ply laminated composite and soft core sandwich plates", *Steel Compos. Struct.*, **33**(5), 663-679. https://doi.org/10.12989/scs.2019.33.5.663.

Semmah, A., Heireche, H., Bousahla, A.A. and Tounsi, A. (2019), "Thermal buckling analysis of SWBNNT on Winkler foundation by non local FSDT", *Adv. Nano Res.*, 7(2), 89-98. https://doi.org/10.12989/anr.2019.7.2.089.

Soltani, K., Bessaim, A., Houari, M.S.A., Kaci, A., Benguediab, M., Tounsi, A. and Alhodaly, M.S. (2019), "A novel hyperbolic shear deformation theory for the mechanical buckling analysis of advanced composite plates resting on elastic foundations", *Steel Compos. Struct.*, **30**(1), 13-29. https://doi.org/10.12989/scs.2019.30.1.013.

Thanh, C.L., Tran, L.V., Vu-Huu, T. and Abdel-Wahab, M. (2019), "The size-dependent thermal bending and buckling analyses of composite laminate microplate based on new modified couple stress theory and isogeometric analysis", *Comput. Method. Appl. M.*, **350**, 337-361. https://doi.org/10.1016/j.cma.2019.02.028.

Tlidji, Y., Zidour, M., Draiche, K., Safa, A., Bourada, M., Tounsi, A. and Mahmoud, S.R. (2019), "Vibration analysis of different material distributions of functionally graded microbeam", *Struct. Eng. Mech.*, **69**(6), 637-649. https://doi.org/10.12989/sem.2019.69.6.637.

Tounsi, A., Al-Dulaijan, S.U., Al-Osta, M.A., Chikh, A., Al-Zahrani, M.M., Sharif, A. and Tounsi, A. (2020), "A four variable trigonometric integral plate theory for hygro-thermo-mechanical bending analysis of AFG ceramic-metal plates resting on a two-parameter elastic foundation", *Steel Compos. Struct.*, **34**(4), 511-524. https://doi.org/10.12989/scs.2020.34.4.511.

Vo, T.P., Thai, H.T., Nguyen, T.K., Lanc, D. and Karamanli, A. (2017), "Flexural analysis of laminated composite and sandwich beams using a four-unknown shear and normal deformation theory", *Compos. Struct.*, **176**, 388-397.

Wang, Y., Zeng, R. and Safarpour, M. (2020), "Vibration analysis of FG-GPLRC annular plate in a thermal environment", *Mech. Based Des. Struct. Mach.*, 1-19. https://doi.org/10.1080/15397734.2020.1719508.

Wattanasakulpong, N. and Chaikittiratana, A. (2015), "Exact solutions for static and dynamic analyses of carbon nanotube-reinforced composite plates with Pasternak elastic foundation", *Appl. Math. Model.*, **39**(18), 5459-5472. https://doi.org/10.1016/j.apm.2014.12.058.

Wu, H., Kitipornchai, S. and Yang, J. (2017), "Thermal buckling and postbuckling of functionally graded graphene nanocomposite plates", *Mater. Design*, **132**, 430-441. https://doi.org/10.1016/j.matdes.2017.07.025.

Zarga, D., Tounsi, A., Bousahla, A.A., Bourada, F. and Mahmoud, S.R. (2019), "Thermomechanical bending study for functionally graded sandwich plates using a simple quasi-3D shear deformation theory", *Steel Compos. Struct.*, **32**(3), 389-410. https://doi.org/10.12989/scs.2019.32.3.389.

Zaoui, F.Z., Ouinas, D. and Tounsi, A. (2019), "New 2D and quasi-3D shear deformation theories for free vibration of functionally graded plates on elastic foundations", *Compos. Part B: Eng.*, **159**, 231-247. https://doi.org/10.1016/j.compositesb.2018.09.051.

Zhang, L.W., Zhang, Y. and Liew, K.M. (2017), "Vibration analysis of quadrilateral graphene sheets subjected to an in-plane magnetic field based on nonlocal elasticity theory", *Compos. Part B: Eng.*, **118**, 96-103.

Zhao, Z., Feng, C., Wang, Y. and Yang, J. (2017), "Bending and vibration analysis of functionally graded trapezoidal nanocomposite plates reinforced with graphene nanoplatelets (GPLs)", *Compos. Struct.*, **180**, 799-808. https://doi.org/10.1016/j.compstruct.2017.08.044.

CC

Appendix

$$S_{1111}=\frac{1}{2\left(1-\mu_m\right)}\left(\begin{array}{l}1-2\mu_m+\dfrac{3\alpha^2-1}{\alpha^2-1}\\-\left(1-2\mu_m+\dfrac{3\alpha^2}{\alpha^2-1}\right)\tilde{J}\end{array}\right) \tag{A1}$$

$$S_{2222}=\frac{3}{8\left(1-\mu_m\right)}\frac{\alpha^2}{\alpha^2-1}+\frac{1}{4\left(1-\mu_m\right)}\left(\begin{array}{l}1-2\mu_m\\-\dfrac{9}{4\left(\alpha^2-1\right)}\end{array}\right)\tilde{J} \tag{A2}$$

$$S_{2233}=\frac{1}{4\left(1-\mu_m\right)}\left(\begin{array}{l}\dfrac{\alpha^2}{2\left(\alpha^2-1\right)}\\-\left(1-2\mu_m+\dfrac{3}{4\left(\alpha^2-1\right)}\right)\tilde{J}\end{array}\right) \tag{A3}$$

$$\begin{aligned}S_{2211}&=-\frac{1}{2\left(1-\mu_m\right)}\frac{\alpha^2}{\alpha^2-1}\\&+\frac{1}{4\left(1-\mu_m\right)}\left(\frac{3\alpha^2}{\alpha^2-1}-\left(1-2\mu_m\right)\right)\tilde{J}\end{aligned} \tag{A4}$$

$$\begin{aligned}S_{1122}&=-\frac{1}{2\left(1-\mu_m\right)}\left(1-2\mu_m+\frac{1}{\left(\alpha^2-1\right)}\right)\\&+\frac{1}{2\left(1-\mu_m\right)}\left(1-2\mu_m+\frac{3}{2\left(\alpha^2-1\right)}\right)\tilde{J}\end{aligned} \tag{A5}$$

$$S_{2323}=\frac{1}{4\left(1-\mu_m\right)}\left(\begin{array}{l}\dfrac{\alpha^2}{2\left(\alpha^2-1\right)}\\+\left(1-2\mu_m-\dfrac{3}{4\left(\alpha^2-1\right)}\right)\tilde{J}\end{array}\right) \tag{A6}$$

$$S_{1212}=\frac{1}{4\left(1-\mu_m\right)}\left(\begin{array}{l}1-2\mu_m-\dfrac{\alpha^2+1}{\left(\alpha^2-1\right)}\\-0.5\left(1-2\mu_m-\dfrac{3\left(\alpha^2+1\right)}{\left(\alpha^2-1\right)}\right)\tilde{J}\end{array}\right) \tag{A7}$$

and

$$\tilde{J}=\frac{\alpha^2\left(\alpha^2-1\right)^{0.5}-\alpha acosh(\alpha)}{\left(\alpha^2-1\right)^{1.5}} \tag{A8}$$